

Joint NASA/DLR Aeronautics Design Challenge 2016-2017

FH Aachen University of Applied Sciences

HORUS 3000-300



Teamleiter

Jan Frederik Bremen, B. Eng. Christian Franke

Akademische Betreuer

Prof. Dr.-Ing. Frank Janser,

Prof. Dr.-Ing. Carsten Braun, Prof. Dr.-Ing. Marc Havermann

Einreichung am 29.06.2017

Abstract

This work contains a conceptual design of a new airplane designed against the requirements of flight path 2035. The main task is the reduction of noise and emissions for a subsonic passenger aircraft.

The result is a mid-size, short range aircraft carrying 300 passengers, having a maximum range of 3000 km and a cruise Mach number of 0.6 at 20,000 ft. It is especially designed for the highly expanding Asian market.

The new designed aircraft has an unswept, tapered wing with a C-Wing and a semi blended body. The fuselage of the semi blended body needs a new cabin configuration driven by the outer shape. Fast boarding and deboarding is a resolved task of the cabin. The two recuperative and intercooled turbo generators for the serial hybrid propulsion system are embedded within the fuselage. Together with a battery, they power the electrically driven ducted fans mounted on the top rear part of the fuselage. With the futuristic propulsion system, the required NO_x reduction is achievable. By running the turbines only at the design point and implementing a lean prevaporized premixed (LPP) combustion chamber, a NO_x reduction of up to 90% can be reached.

Even without comprehensive aerodynamic optimizations the configuration reaches a maximum L/D of 17. Various recently carried out studies reveal possible L/D ratios of 25 to 30 with this kind of configuration. To meet the noise reduction requirements, the primary and secondary control surfaces are built in morphing structures resulting in a gap-free assembly.

Furthermore, to reduce the noise emissions emitted by the landing gear during the final approach and takeoff, a new automatic pull out landing gear is included.

Table of contents

1	Introduction.....	1
2	Aerodynamics.....	2
2.1	The Fuselage	2
2.2	The Wing	2
2.3	The C-Wing.....	2
2.4	Design	3
2.5	Aerodynamic results	5
3	Flight Performance	6
3.1	Matching Diagram.....	6
3.2	Empennage Layout & Sizing.....	7
3.2.1	Empennage Configuration.....	7
3.2.2	Initial Weight and Drag Estimation.....	7
3.3	Flight Performance Calculation	8
4	Propulsion.....	10
4.1	General.....	10
4.2	Flight Mission	11
4.3	Dimensioning	12
4.4	Components of the Propulsion System.....	12
4.4.1	Fan	12
4.4.2	Turbo generator	14
4.4.3	Electric System	14
4.4.4	Battery	14
4.5	Emission Reductions	15
4.5.1	Gaseous Emissions	15
4.5.2	Noise Emissions	16
5	Cabin and Systems.....	17
5.1	System Weight and Electrical Consumption Estimation	17
5.2	Landing Gear: Weight and Drag reduction	17
5.3	Single Pilot Operation	18
5.4	Cabin, In-Flight Entertainment and Cabin Crew.....	19
5.5	Electric taxiing.....	20
5.6	Environmental Control Unit	20
6	Weight and Balance.....	21
6.1	Wing Structure	21
6.2	Fuselage Structure	21
6.3	CG and MTOM Calculation.....	22
7	Conclusion	23

List of figures

Figure 1: Aircraft Model 1	4
Figure 2: Aircraft Model 2	4
Figure 3: Process Flow Chart	4
Figure 4: Aerodynamic Results	5
Figure 5: Matching Diagram	6
Figure 6: v-n Diagram, Flight envelope.....	8
Figure 7: Alternative Aviation Fuels [11]	10
Figure 8: Schematic Structure of the Propulsion System	11
Figure 9: Ducted fan station definition [13]	12
Figure 10: FPR-Ma-field, CR-fan achieved significant benefits compared with the SR-fan [14].....	13
Figure 11: Fuel burn over nozzle area	13
Figure 12: Global air traffic CO ₂ emissions roadmap.....	15
Figure 13: 2025 BWB-0009A GTF [32].....	16
Figure 14: Noise Diagram [32].....	16
Figure 15: Cross section of the cabin	19
Figure 16: LED Screens and Seats (lower-deck).....	20
Figure 17: Three view drawing	23

List of tables

Table 1: Flight Path Requirements	1
Table 2: Design Parameters.....	4
Table 3: Typical flight mission data	11
Table 4: Required power and energy for the different flight segments.....	12
Table 5: Assumptions for fan design	13
Table 6: Specific power and efficiency of the components [23]	14
Table 7: Battery cell data.....	15
Table 8: Weight of different aircraft systems.....	17
Table 9: Calculation Center of Gravity.....	22

Nomenclature

α	= angle of attack	n	= load factor
Λ	= Aspect ratio	M	= Mach number
CG	= center of gravity	c_m	= moment coefficient
c_D	= drag coefficient	PAX	= persons approximately
FPR	= fan pressure ratio	S_w	= reference area
FL	= flight level	SPO	= single-pilot-operations
c_{Di}	= induced drag coefficient	$C_{H/V}$	= tail volume coefficient
c_L	= lift coefficient	T/O	= take off
L/D	= lift to drag ratio	v	= velocity

1 Introduction

In a first step, a flight mission was selected. The new aircraft operates at a maximum range of 3000 km and carries 300 passengers. This region is currently not covered in the seat range diagram of all existing aircraft. According to the current flight traffic, the average distance of today's busiest flight routes is about 600 km per flight [1]. Furthermore, the main hubs are working to capacity. For this reason, the number of T/O and landings has to be reduced. Another advantage of this is that the total noise emission would be decreased, because fewer aircraft are required. To enter the Asian market successfully, the maximum range was selected as the longest distance between the main hubs in the Asian market.

The low Mach-number (M) of 0.6 has advantages in emission and noise. The impact of the slow flying aircraft on the total air traffic is a problem. The lower cruising speed compared to recent aircrafts does not have a big impact on the total flight time because the ratio of the cruise flight segment compared to the total trip length is reduced due to the short range. It is more important to have good climb performance because of the short flight distances and noise emissions.

The service ceiling is a result from the M-altitude diagram. It is aerodynamically efficient to fly at flight level (FL) 200 and $M = 0.6$.

The Aircraft should take over the task of a bus or train in this market. Just a very small cargo department is necessary for the short haul flights which results in faster boarding and better ground handling qualities.

Moreover, to reduce weight, the aircraft is built from fiber composite materials. These materials provide a smooth surface for low skin friction. Antennas should be inside the aircraft to reduce interference drag.

Another measure to reduce the noise emissions is to implement an engine shielding. The Aircraft is designed against the following requirements for flight path 2035:

Table 1: Flight Path Requirements

Technology Benefits	Technology Generations (Technology Readiness Level = 4-6)		
	short-term 2015-2025	medium-term 2025-2035	long-term after 2035
Nois (cum maring rel. to Stage 4)	22-32 dB	32-42 dB	42-52 dB
LTO Nox Emission (rel. to CAEP 6)	70-75 %	80%	> 80 %
Cruise Nox Emissions (rel. to 2005 best in class)	65-70 %	80%	> 80 %
Aircraft Fuel/Energy Consumption (rel. to 2005 best in class)	40 - 50%	50 - 60%	60 - 80%

2 Aerodynamics

After a rough conservative mass estimation of the aircraft, the outer shape of the aircraft was determined iteratively.

With the aircraft requirements of a semi-blended, straight wing with a C-Wing wingtip, a lifting fuselage, and a Mach of 0.6 at FL 200, the first sizing of the aircraft was carried out.

2.1 The Fuselage

Some recent studies reveal that the lifting body can carry about 20-30% [2] of the total weight of the aircraft, with a semi-lifting body carrying up to 20% of the total weight. This configuration promises some advantages and is possible to construct in 2035.

The primary task of the fuselage is to carry passengers and systems at low drag. The lifting body provides enough space for passengers and systems, while the shape depends on the number of passengers per row and the height of the cabin.

One advantage is the reduction of wetted area, resulting in a reduction of the total friction drag. To generate as much lift as possible with the fuselage, a high number of seats per row is preferred. Another factor, which is defining the width of the fuselage, is passenger comfort in terms of angular accelerations during roll movements of the aircraft.

The secondary task for the fuselage is to carry the overall weight. For a good result, the induced drag c_{Di} of the fuselage must be optimized. Therefore, the fuselage profile should be symmetric with zero c_{Di} in cruise flight or a profile with a $c_{L0} = 0$.

Furthermore, it is possible to integrate a horizontal stabilizer in the trailing edge.

2.2 The Wing

The wing is unswept to get as high lift as possible at lowest drag. Because of the low M of 0.6, a sweep is not necessary, since the transonic drag rise does not occur if M_{cr} is not reached on top of the wing. It is possible to reduce the pitching moment of the whole aircraft with a sweep angle up to 10 degrees without losing that much lift. The wing carries the rudders, but they should be built as morphing structures [3].

Moreover, the wing should have a laminar profile and additionally a laminar flow control (LFC). Laminar profiles are possible because of the low M and the low attachment line instability due to the unswept wing. The boundary layer suction promises very high c_L values for takeoff and landing. High lift devices are shaped in such a way that no gaps between the surfaces exist in order to reduce noise.

Another point is the high specific rigidity of this wing configuration. It is necessary to reduce the flutter behavior of the implemented C-Wing.

2.3 The C-Wing

The shape of a C-Wing was found using an algorithm which had the purpose of optimizing a nonplanar wingtip configuration for the lowest total drag. This configuration has strong advantages at high c_L values. Therefore, these benefits especially come into effect during climb, T/O and landing and decrease the induced drag

dramatically [4]. This is of particular importance for the presented aircraft, since the ratio of these three flight phases to cruise becomes higher the shorter the range becomes.

Another advantage is the load and bending moment reduction of the wing resulting from the weight of the C-Wing. The bending moment is reduced further due to the down and side force of the upper and the vertical part of the wing, respectively.

This configuration increases the dissipation rate of the wake vortices, making it is possible to increase the number of T/O and landings per hour at airports. Moreover, another important advantage is the possibility to build a tailless aircraft [5].

Several papers explain the benefits of the nonplanar configuration and compare the C-Wing with various winglets or a planar configuration. A 3% total drag reduction in cruise by an increase of the wing mass of 20-30% can be indicated compared to a wingtip [4]. The shape of the C-wing has to be determined in an optimization process for the whole flight mission [6, 7].

2.4 Design

The biggest challenge was to determine a factor for the ratio of the lift-coefficient of the fuselage to that of the wing for this special configuration. Some studies were conducted for semi-blended wing and blended wing bodies, which outlined among others this ratio. However, for these aircraft requirements as a whole, with the straight wing and the C-Wing section, no reference values existed so new calculations must be carried out. To determine which fuselage and wing shapes as well as the connection of the two are best in terms of aerodynamic efficiency, structural weight and system integration, numerical fluid dynamic tools are used.

For the given air properties at FL 200, the necessary $c_L \cdot S_w$ was calculated according to the equation:

$$L = \frac{\rho}{2} v^2 c_L \cdot S_w$$

A fuselage wing lift ratio is chosen such that the fuselage will carry 20% of the total weight [2]. The average mass of the aircraft during cruise is calculated with the following equation.

$$m_{cruise} = \frac{MTOW + 0,9 \cdot MTOW}{2}$$

To find out an optimal solution in time, different airfoils for the wing and fuselage were analyzed during the design process. The open source program Surface Modeler Sumo© was used to generate new aircraft configurations in a straightforward way. After creating a solid in CATIA V5© the aircraft is analyzed aerodynamically with FlightStream© from Research in Flight. The CFD-solver is based on the panel method, hence it is capable of computing the pressure distribution and the velocities for an arbitrarily shaped object, thereby predicting the lift and induced drag values quite well. Additionally, the software provides an approximation for friction and pressure drag. An analytical approximation for the viscous drag of the fuselage and wing [8] shows a good accordance with the software results. The advantages of the panel solver are the speed of the calculations in terms of computational and human work load as well as the ability to analyze arbitrarily shaped bodies.

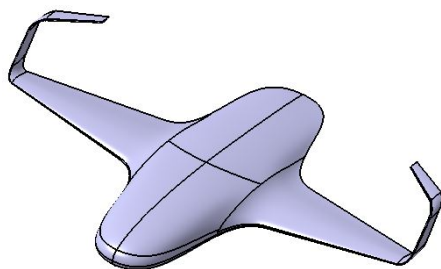
Additionally, a comparison of a fuselage-wing and fuselage-wing-C-wingtip configuration was done to analyze the benefits of the C-wing.

After the first results, it became obvious that the first approach of an elliptically shaped slender lifting fuselage in combination with an elongated center wing fairing is not efficient due to a very high induced drag of the lifting fuselage and a low lift-coefficient ratio of the fuselage of 8%. Therefore, a more blended configuration is mandatory.

The wing is built with a NACA 64-515 profile, which can have a laminar flow over 40% of the chord length and a design c_L of 0.5, while the fuselage has a symmetric NACA 0015 profile, which has no induced drag for $\alpha = 0^\circ$. Symmetric NACA 0013-0009 profiles are used for the C-Wing, since aerodynamic washout and the smaller airfoil reduce drag.

Table 2: Design Parameters

Parameter	Value	Unit	Parameter	Value	Unit
S_{ref}	248	m^2	Taper ratio	6.4	-
Span	50	m	Taperratio w. C-Wing	10.67	-
C_{MAC}	4.96	m	Aspect ratio Λ	10.08	-
Lifratio fuselage	0.2499	-	Aspect ratio w. C-Wing	17.71	-
Design C_L of Wing	0.523	-	Dihedral angle	3	$^\circ$
Design cruise C_L	0.37	-	Sweep Angle	0	$^\circ$
Angle of incidence	5	$^\circ$	Twist	-2	$^\circ$



To get even better aerodynamic results Model 2 (Figure 2) was introduced with new airfoils and a sweep of 10° . The fuselage is built with an HQs 1.5-3 cmo-0 profile. It has the same thickness as the NACA 0015. However, it is an S-Shape airfoil resulting in better static stability. For the wing, an E216 airfoil is used, which is optimized for the cruise conditions at $M = 0.6$.

```

graph LR
    A[Input requirements: M, H_cruiser, W_estimated straight tapered wing] -- "Atmospheric Model Assumption: Lifratio 0,2 (Paper)" --> B[Prediction for a c_l · S_W]
    B -- "Design c_l = 0,5" --> C[Calculated Wingarea S_W]
    C -- "Generate Model with C-Wing" --> D[Calculation in FlightStream]
    D -- "Output: c_l, c_d, c_m, Lifratio" --> E[Variation of Fuselage, C-Wing and Wing connection]
    E -- "Repeat multiple times to find best Lifratio" --> F[New Lifratio]
    F --> A
    E --> G[Resize Wing (and include vertical and horizontal Tailplane after sizing of Engines)]
    G -- "Give data to Masses and Loadings to compute new MTOW" --> H[Outer Iteration Loop Change of MTOW]
    H --> A
  
```

The flowchart illustrates an iterative design process for a wing. It begins with input requirements (mass, height, estimated wing area) and an atmospheric model assumption. The process involves predicting lift, calculating wing area, generating a model, and performing calculations in FlightStream. The output is used to vary the fuselage, C-wing, and wing connection, which then feeds back into the input requirements to find the best lift ratio. Additionally, the process includes resizing the wing and updating the mass and loadings to compute a new MTOW, which also feeds back into the input requirements.

FH Aachen

2.5 Aerodynamic results

The main results of the analysis are displayed in the diagrams in Figure 4. All the results are based on a constant M of 0.6 and the properties of air at FL 200. The reference area for the Model 1 and the model without C-Wing is 248 m^2 while the Model 2 has a reference area of 230 m^2 . All results were generated with FlightStream, hence the results for higher angle of attack (α) and c_L values exceeding 1.5 are inaccurate because the panel method is not able to capture stall prediction. Moreover, as mentioned above the simulation provides a good prediction for c_{Di} and an approximation for c_{D0} , but the simulation models do not include the vertical- and horizontal stabilizer as well as the nacelles. Therefore, the drag estimation of the empennage in Section 3.2.2 as well as another drag estimation for the nacelles according to Raymer [8] giving a drag coefficient of $c_{D0,N,V,H}=0.0041$ are added to the total drag of the aircraft.

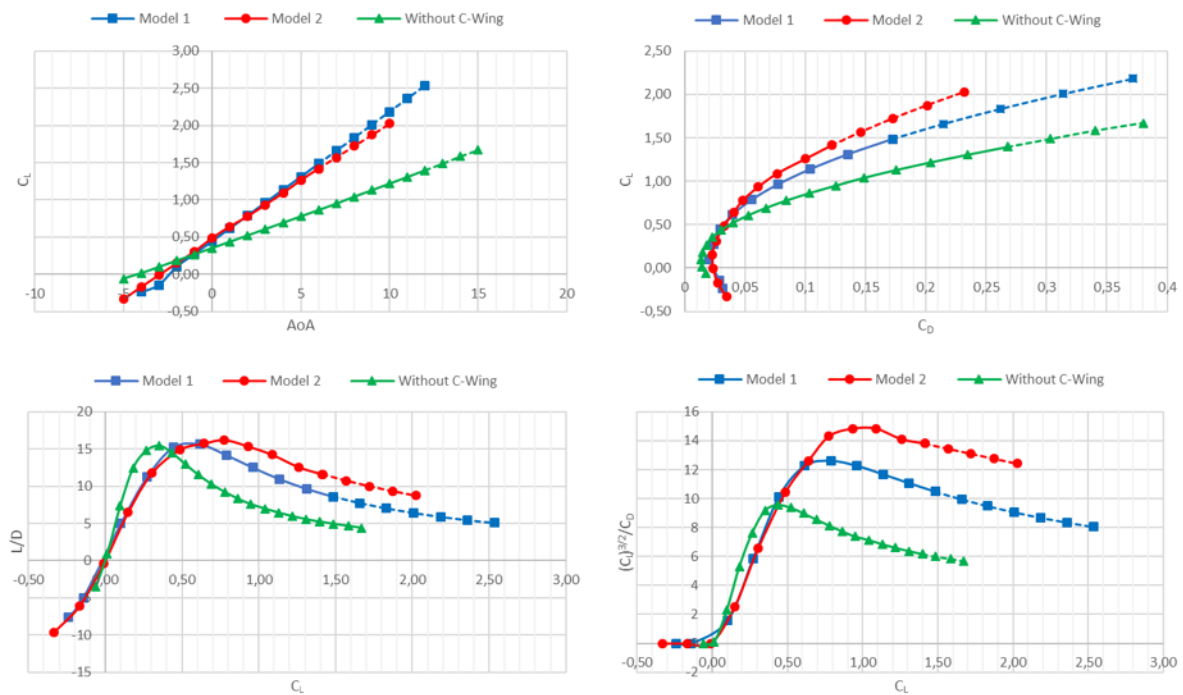


Figure 4: Aerodynamic Results

The aerodynamic benefits of the C-Wing and Model 2 are clear. Comparing Model 1 with the C-Wing to the same configuration without the C-Wing, the c_L/α slope as well as the climb rate are notably higher. The c_L - c_D -diagram indicates that the c_{D0} for the model without the C-Wing is smaller due to the missing additional viscous drag of the C-Wing, while the induced drag c_{Di} is greater than that of Model 1. Especially for higher c_L -values during takeoff and climb, the difference is more significant.

Comparing Model 1 with Model 2, even better results can be achieved. As is evident from the diagrams that the c_L/α slope as well as the L/D below a c_L -value of 0.4 are nearly the same, but for higher c_L -values the induced drag is reduced further. This causes a significant increase of the climb rate for higher c_L -values. In further aerodynamic optimization studies, the maximum L/D can be increased further up to 25 [2] and shifted more to the design c_L of about 0.5. To get meaningful results, the further calculations based on L/D -value of 25. This characteristic is received by shifting the polar.

3 Flight Performance

3.1 Matching Diagram

At the beginning of the design process some aircraft parameters must be estimated to make further calculations possible, a so called preliminary sizing has to be performed. This can be done by a method introduced by Laurence L. Loftin Jr., the so-called Matching Diagram. With some assumptions based on the airport and cruise requirements, the thrust-to-weight ratio and the wing-loading can be estimated. The landing and takeoff field lengths, the second climb segment, the missed approach, and the cruise flight must therefore be analyzed.

In the first step, the landing field length is investigated; therefore, an assumption of the maximum landing lift coefficient was necessary. Based on statistical values, a $C_{L,max,L}=3.0$ was chosen. Furthermore, a landing field length and a landing-to-takeoff-mass-ratio had to be determined. The developed aircraft is a large short haul aircraft, so the mass-ratio was defined to 0.91 which is a good statistical value for this class of aircraft. The aircraft should be capable to serve every airport which can be served by an Airbus A320 so the landing field length was selected as 1500 m, which is nearly the same as the minimum landing field length of an A320.

In the second step, the takeoff field is examined. A takeoff field length and a maximum takeoff lift coefficient was needed here. The takeoff field length was defined to 2000 m, which is slightly shorter than that of the A320, and the maximum takeoff lift coefficient was estimated to $C_{L,max,TO}=2.5$.

In the next step, the second climb segment is analyzed, where the wing aspect ratio and the number of engines must be known. First aerodynamic calculations delivered a preliminary aspect ratio of $\Lambda=10.9$. The number of engines was determined to be two.

In the last step, the climb after a missed approach is analyzed. The required input parameters are the maximum landing lift coefficient, the wing aspect ratio, the number of engines, and the landing-to-takeoff-mass ratio. All these values have been defined in the previous steps. Whether the landing gear is retracted or extended must also be defined. For the presented analysis, a retracted landing gear was chosen because of the premeditated integration of an automated landing gear system, which will retract the landing gear immediately after the decision to perform a go-around (see Section 5.2).

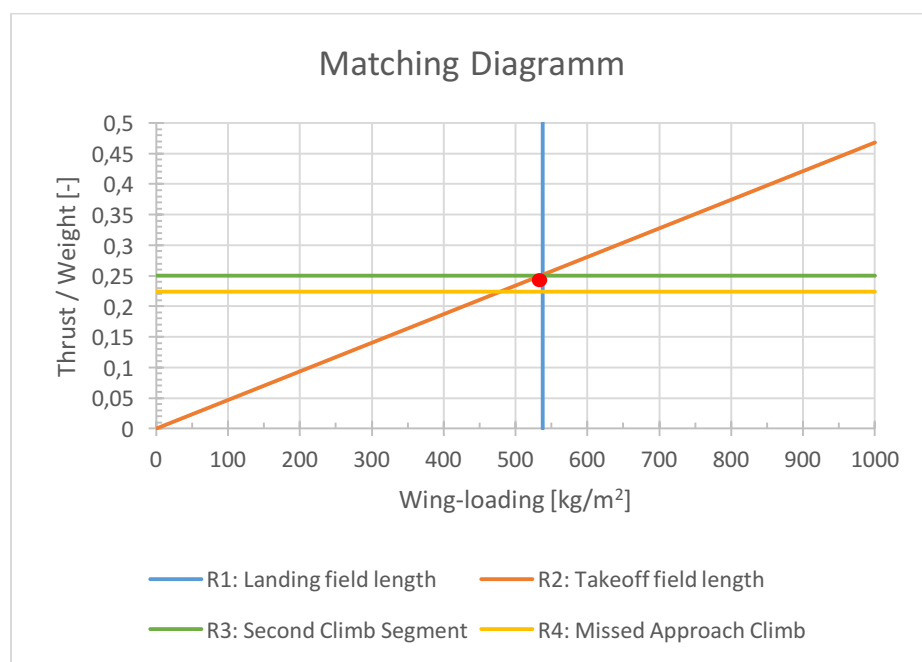


Figure 5: Matching Diagram

The results of the four steps are depicted in the Matching Diagram in Figure 5, which shows the thrust-to-weight-ratio versus the wing-loading. The point of the lowest thrust-to-weight-ratio, which delivers smaller engines, and the highest wing loading, which provides the smallest wing surface, is chosen as the design point. The design point delivers a thrust-to-weight-ratio of 0.25 and a wing-loading of 540 kg/m², indicated by a red circle in Figure 5.

3.2 Empennage Layout & Sizing

The purpose of the Empennage is to provide stability, controllability, and trimmability for all flight situations and conditions. The empennage of an aircraft contains the horizontal stabilizer with the elevator and the vertical stabilizer with the rudder.

The principle task of the empennage is to ensure that the aircraft is stable. It can be distinguished between static and dynamic stability. Static stability means that the aircraft generates a moment that moves the aircraft back to its original flight state after a disturbance. Dynamic stability means that the oscillating movement caused by a disturbance is damped.

The control surfaces vary the lift of the stabilizers to create moments around the center of gravity, thus the aircraft becomes controllable. It must be ensured that the empennage is suitable to generate enough control power to achieve the desired maneuverability in each flight state with moderate control forces. Another important function of the empennage is to ensure that the aircraft can be trimmed in flight states that must be maintained for a longer period.

For the presented conceptual design, an empennage sizing with respect to static stability and trim requirements was performed. Further analysis like a stability and control analysis has to be performed in later stages of the design process.

The requirements for the longitudinal static stability are a negative slope of the $C_{m,c.g.}$ versus α , which means that the center of gravity has to be in front of the aerodynamic center of the whole aircraft, and a positive lift-independent moment coefficient $C_{m,0}$. So the flight mechanical behavior of the aircraft is determined by the position of overall aerodynamic center, the center of gravity and by the size and location of the empennage.

3.2.1 Empennage Configuration

For the developed design, there are two components used to ensure static stability: the C-wing and the tail of the lifting body. The upper part of the C-Wing generates downforces. This reduces the bending moment of the wing but also shifts the aerodynamic center toward the rear of the aircraft, resulting in a significantly smaller horizontal stabilizer surface which is needed to provide the required static stability. The tail of the lifting body fuselage is used as horizontal stabilizer surface and for propulsion integration.

The layout of the empennage was dictated by the integration of the fans. A U-Tail Configuration was selected because of the required space for the fans and the noise shielding effect of the two vertical stabilizers. The slightly increased interference drag of the U-Tail is acceptable.

For the empennage, the symmetrical airfoil NACA 0012 was selected. Aspect ratios of four and two were defined for the horizontal and vertical stabilizers, respectively.

3.2.2 Initial Weight and Drag Estimation

To provide initial values for the weight & balance and aerodynamic calculations, a rough weight and drag estimation was performed. The empennage surface was estimated by the tail volume approach. According to

Raymer [9], for the horizontal stabilizer surface a tail volume coefficient $c_H = 1.0$ is a good statistical assumption. Due to the special configuration with the C-wingtip the coefficient was reduced to $c_H = 0.7$. This delivers a horizontal stabilizer surface of 52 m².

For the vertical stabilizer, Raymer [9] suggests a tail volume coefficient $c_V = 0.09$. For the presented design, a coefficient of $c_V = 0.07$ was chosen because of the large wing tip fence of the C-wing configuration, delivering a vertical stabilizer surface of 54 m².

With the estimated surfaces, a Class II weight estimation for transport aircraft according to Raymer [9] was performed. The ultimate load factor was assumed with 3.75 without respect to gusts. This delivers a weight of about 2.000 kg.

For the estimation of the lift-independent drag, a drag estimation according to Raymer [9] was performed. It was assumed that the flow on the empennage is fully turbulent. The form factor FF was calculated with the parameters of the chosen airfoil NACA 0012 and the interference drag factor for a U-Tail-Configuration was determined to be 1.04 [9]. The analysis delivers a value for $c_{D,0} = 0.0036$.

Sizing for trim conditions does not affect the surface areas so much, due to the small lever arm in the one engine inoperative condition for the vertical tail. For the horizontal tail, the aerodynamic optimization gave better moments along with the effect of the upper part of the C-wing, and so the previously sized areas were used for the start of the design.

3.3 Flight Performance Calculation

For the structural design, a v-n-diagram is necessary to calculate the weight loads. According to the certification specifications for large airplanes (CS-25), maximum limit load factors of +2.5/-1 was defined for velocities between v_C and v_A . For this step, the cruise velocity is needed, which is depending on the cruise altitude. With the results from aerodynamic simulations, the best cruise altitude was determined to be FL 200. With the corresponding maximum lift coefficients, the diagram could be calculated completely (see Figure 6).

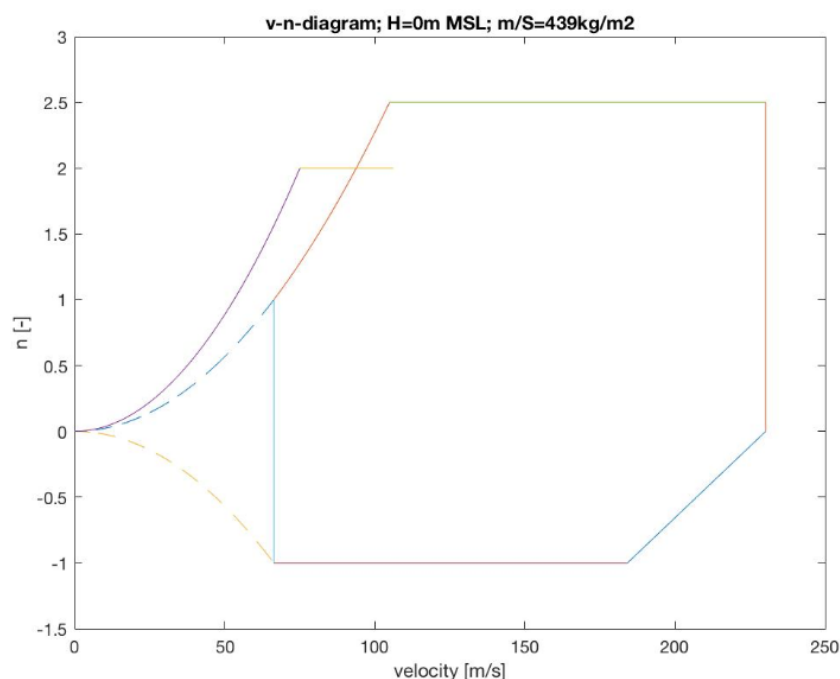


Figure 6: v-n Diagram, Flight envelope

For the extended high lift devices, the prescribed maximum lift factor of 2.5 was assumed. Safety margins are according to CS-25.

With the results from the matching diagram an initial value for the required thrust could be determined. First iterations could be done with the thrust-to-weight ratio and the power necessary to achieve the required climb gradients in the certification specifications. With this result a more detailed design of the aircraft's fans and power plant could be done.

4 Propulsion

4.1 General

The need for a clean and reliable future propulsion concept is one of the main drivers for next generation aircrafts. According to the requirements, the propulsion system was developed in parallel under four distinct categories: noise, landing and T/O NO_x emissions, Cruise NO_x emissions and aircraft fuel/energy consumption. The first technology benefit that had to be achieved is reduction to 50-60% aircraft fuel/energy consumption compared to the best version in 2005. The second technology benefit is a significant reduction of the NO_x emissions during a landing and takeoff cycle and during cruise compared to CAEP6 and the best version in 2005. This should be done primarily with the propulsion system of the aircraft. To reduce the noise level to 32-42 dB, a clever engine design needed to be developed.

The cleanest aircraft propulsion system would be purely electrical, driven by electric motors and a huge battery system. The energy that is stored in the battery would come only from renewable energy sources. That would result in a gaseous emission free propulsion system. The problem with such a system would be the specific volumetric energy density. The gravimetric energy density and the volumetric energy density are low for such systems as shown in Figure 7. The required power that is needed to operate the aircraft would lead to heavy battery packs and therefore to an inefficient, heavy aircraft.

To fly with an alternative fuel like hydrogen would not be an option either because new fuel storage systems would need to be developed, tested, and certified. Like shown in Figure 7, hydrogen has a high gravimetric energy density at a low volumetric energy density compared to contemporary energy sources. Hydrogen has no CO₂ emissions, but during its combustion it produces NO_x and water vapor. Existing studies have shown that the resulting formation of clouds occur due to water vapor has a strong negative impact on the climate [10].

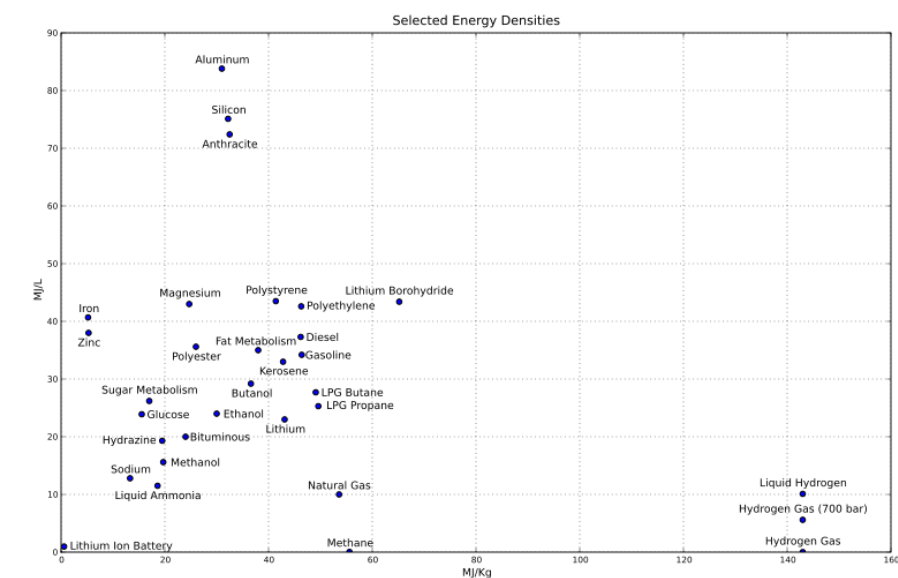


Figure 7: Alternative Aviation Fuels [11]

To get the benefits of the high gravimetric energy density at a high volumetric energy density, a low CO₂ life cycle emission, a reduction in NO_x, and no change of existing fuel systems, bio fuel produced from algae is the best future solution for the primary energy source. The fact that the fuel is produced from algae leads to a low life cycle CO₂ because the algae uses almost the same amount of CO₂ for growing as it produces during

combustion [12]. To reduce additional high development costs, bio fuels can be used with the existing fuel system technologies and their implementation in the aircraft.

The choice of bio fuel as the primary energy source leads to engines with combustion processes. The main problem for engines with combustion processes is the fact that only one design point exists in which it runs at its highest efficiency and lowest emissions. But to fulfill a flight cycle of the aircraft, the engines need to run at different off-design points to provide different thrust and therefore at different efficiency and emission levels. To stay in the most efficient design point during one flight cycle, the engines need to be decoupled from the fans and an energy buffering system needs to be implemented. This is done by a serial hybrid propulsion system as shown in Figure 8.

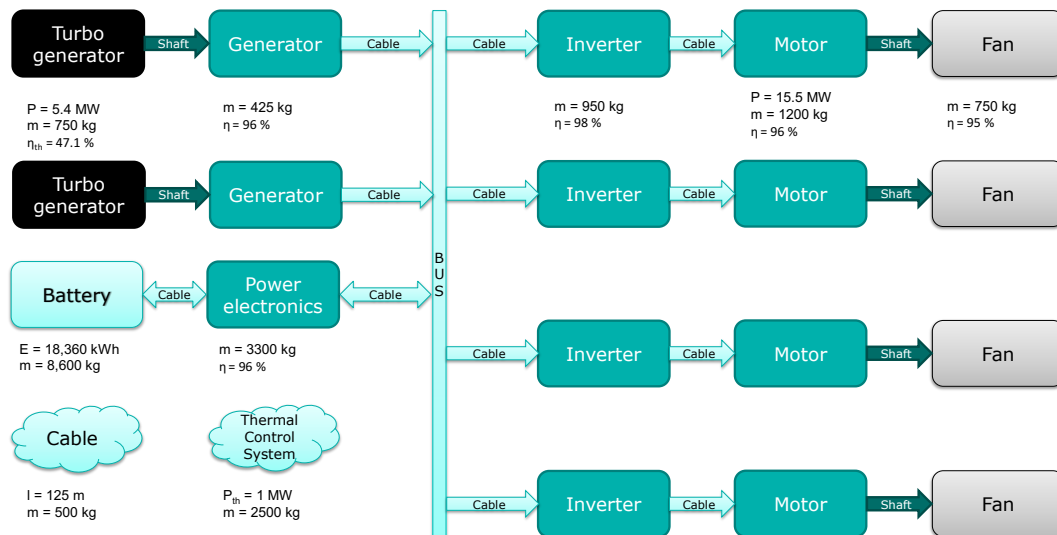


Figure 8: Schematic Structure of the Propulsion System

Four electric motors will power four ducted fans. Two recuperative and intercooled turbo generators produce constant shaft power of 5.4 MW each, which is converted to electric power via two generators. For takeoff and climb additional power is needed, which can't be provided by the gas turbines due to the described problem. To accomplish this, battery packs are installed, which deliver the additional power during this flight segments.

4.2 Flight Mission

The first step while sizing the propulsion system is to set up the requirements. Initially an ordinary flight mission has to be set up for which the propulsion system has to be optimized. Thereafter, it must be checked if the propulsion system can meet all special condition requirements, such as hot-and-high and one engine inoperative conditions.

Due to the requirements described in Section 4.1, the flight mission in Table 3 is set up as the typical one. The thrust and the velocity of the different flight segments arise from the required flight performance and are the basis for designing the propulsion system. These are summarized below in Table 3.

Table 3: Typical flight mission data

Flight segment	Details	Required thrust [kN]	Velocity [m/s]
Take off	Thrust-to-Weight-ratio = 0.297	323	64
Initial climb	Till 2000 ft above airport attitude	323	64
Climb	Till FL 200	138	118
Cruise	2800 km at FL 200	36.5	160
Descend	1000 ft/min sink rate	0	134
Loiter	10 min at 5000 ft	41	105

As special condition requirements, hot-and-high conditions for takeoff at an elevation of 2000 m above MSL are considered. These are limiting conditions for the dimensioning of the fans, motors, and the battery (due to the maximum current can take out of the battery). The one engine inoperative condition (OEI) is covered with the thrust-to-weight-ratio given by the matching diagram. The ratio is calculated for a conventional 2 engine aircraft; for the proposed concept, it is considered that two fans and one turbo generator fail at the same time.

4.3 Dimensioning

To size the components of the propulsion system, the thrust and velocity of the different flight segments shown in Table 3 were used. From this, the total power that is needed to drive the fans was calculated (see Section 4.4.1). For the electrical power consumption of the cabin and systems, 500 kW are estimated for all flight segments (see Section 5.1). With the efficiency of the motors, the total electric energy needed for different flight segments were calculated (listed in Table 4). The average power of the whole mission is 10.8 MW, so the turbo generators were sized to exactly this power. Each turbo generator performs at a constant power of 5.4 MW. The energy difference between the required energy and the energy provided form the turbo generators has to be provided by the battery. This led to a minimum battery capacity of 4030 kWh.

Table 4: Required power and energy for the different flight segments

Flight segment	Duration [h:min:sec]	Required power for the fans [MW]	Total Required Energy [kWh]	Required Energy from battery [kWh]
Take off	0:00:22	62	316	258
Initial climb	0:00:41	62	706	595
Climb	0:09:00	31	4,651	3.178
Cruise	3:46:00	9.6	45,912	-981
Descend	0:20:00	1	484	-2.790
Loiter	0:10:00	8.3	1,377	-260

4.4 Components of the Propulsion System

4.4.1 Fan

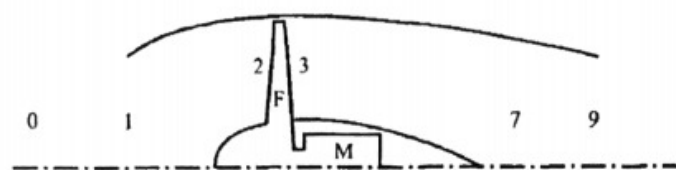


Figure 9: Ducted fan station definition [13]

Ducted fans, shown in Figure 9, have the best capability to avoid noise emissions, although unducted fans could lead to another gain in efficiency. A counter rotating fan leads to significant gains in efficiency for high M at high fan pressure ratios [14]. The cruise M is low compared with today's aircrafts ($M_{\text{cruise}} = 0.6$). Furthermore, a low fan pressure ratio (FPR) of 1.25 at cruise, as well as the lower complexity of the single rotating fan, led to the decision not to use a counter rotating fan. The fan is designed as a variable pitch fan, to avoid fan stall due to the low FPR and achieve a high efficiency over the whole operating range.

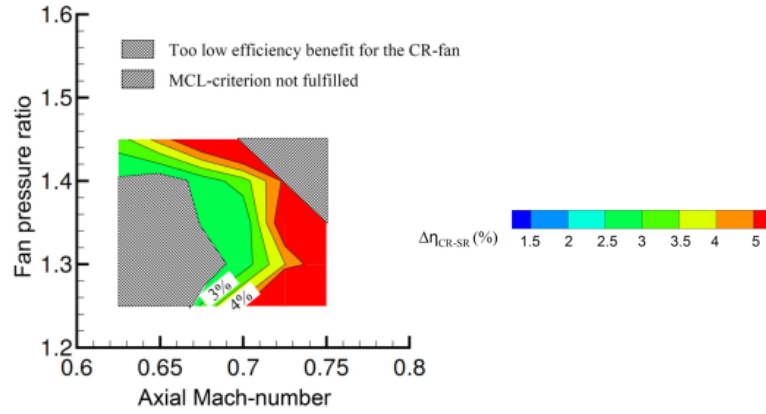


Figure 10: FPR-Ma-field, CR-fan achieved significant benefits compared with the SR-fan [14]

The fans are integrated in the rear section on top of the fuselage so they ingest the boundary layer from the top side of the fuselage (pictures in Appendix). This boundary layer ingestion results in a non-uniform disturbed flow at the fans. According to [15] this leads to a reduction of isentropic fan efficiency of around 1-2% relative to operation with a clean inlet. But by ingesting the boundary layer with lower flow velocities than the free stream, the propulsion efficiency is improved. This leads to an 8 % reduction in total drag. [16]

Lower FPR reduces the jet exit velocity, which improves propulsive efficiency, but also dramatically decreases the shaft speed. NASA research results show that the maximum shaft speed of FPR above 1.5 is too high and makes the direct electric motor drive impossible. FPR below 1.2 is also not attractive because of difficulty to recover inlet duct pressure loss. [17] The FPR of the proposed propulsion system should be from 1.2 to 1.5. This leads to non-choked fan nozzles over the whole operation range.

During the fan design process, the following assumptions were made:

Table 5: Assumptions for fan design

Quantity	Description	Value
M_2	Fan axial Mach-number	0.5
π_{inlet}	Inlet total pressure loss	0.998 [18] [19]
$\pi_{3,7}$	Fan – nozzle total pressure loss	0.995
η_{nozzle}	Isentropic nozzle efficiency	0.997 [18]
η_{fan}	Isentropic fan efficiency	0.95 [18] [19]

With a given thrust and free-stream velocity, fan areas can be calculated by specifying a fixed nozzle area A_8 . To find the optimum nozzle area, the flight mission from Section 4.2 is assumed. With the efficiencies of all components of the propulsion system, the fuel burn per 100 km per PAX can be calculated depending on the nozzle area, shown in Figure 11.

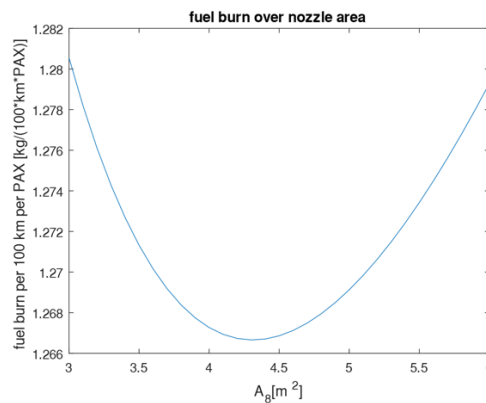


Figure 11: Fuel burn over nozzle area

This optimization leads to a total nozzle area A_8 of all four fans from 4.3 m^2 and a total fan area A_2 of 6.5 m^2 . The FPR comes within the limits from 1.2 to 1.5, which is exactly the acceptable range described in [17].

4.4.2 Turbo generator

This aircraft uses two recuperative and intercooled turbo generators. These produce constant shaft power and run at their design point during the whole flight. This means the engines can be optimized only for this operation point (i.e. the combustion chamber temperature can be set to the optimal compromise between CO and NO_x emissions). To reduce NO_x by about 90%, an LPP (lean prevaporized premixed) combustion chamber is integrated in the engines [20]. All components must be sized not for peak power during takeoff and climb, but for the lower constant power, which leads to lower weight.

For conventional turbofan engines, it is difficult to integrate an intercooling and exhaust gas heat exchanger because the required space for the additional components increases outer dimensions. This problem is avoided in the proposed concept by integrating the engines inside the fuselage. Only an inlet duct and a jet outlet affect the outer shape of the aircraft. The recuperator of the intercooling is placed between the fan and the nozzle, which leads to some additional thrust.

According to [21], future recuperated turboshaft aeroengines can reach a specific fuel consumption up to $0.3 \text{ lb}/(\text{hp}\cdot\text{hr})$ with a specific weight greater than $5 \text{ hp}/\text{lb}$. With a heating value of Jet A-1 of $42.8 \text{ MJ}/\text{kg}$ a thermal efficiency of 46 % is reached at a specific weight of $8.2 \text{ kW}/\text{kg}$. [22] reached a thermal efficiency of 47.1 %.

4.4.3 Electric System

The electric system of a hybrid aircraft is different to regular aircraft models. It is therefore important to identify which parts are needed for a hybrid aircraft. With this comparison, it was possible to identify the following parts as indispensable: generator, motor, inverter, cables, and thermal management systems.

The schematic structure of the electrical system from this aircraft is shown in Figure 8. Research shows that it is not likely to have superconducting electrical systems by 2035, which leads to a non-superconducting electrical system [23]. The specific power and efficiency of the components quoted in [23] are listed in Table 6. To reduce cable heat losses, high voltage electric motors are used operating at 3kV DC.

Table 6: Specific power and efficiency of the components [23]

Component	Specific Power / Specific Weight	Efficiency
Generator	13 kW/kg	96 %
Motor	13 kW/kg	96 %
Inverter	16.5 kW/kg	98 %
Cable	3.9 kg/m	99.6 %
Thermal management system	0.68 kW(th)/kg	

4.4.4 Battery

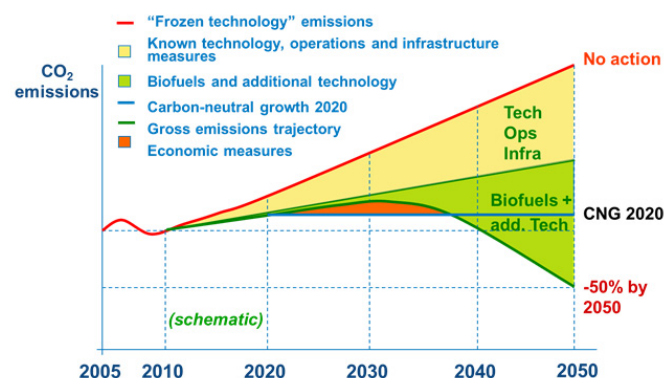
To store the required energy that is needed to generate the additional power during takeoff and climb, a battery pack is installed. Today, battery technology is not capable of efficiently storing a huge amount of energy with respect to low weight. The gravimetric energy density of today's most efficient battery cells is just above $300 \text{ Wh}/\text{kg}$ ('Panasonic 2170' developed for Tesla, Inc. [24]) [25]. But in 2035 battery cells will reach energy densities of $600 \text{ Wh}/\text{kg}$ [26], which will make them a lot lighter and therefore efficient to use in propulsion systems [27]. Battery cells also have a limited amount of recharge cycles. At the moment, high power battery cells only last

for a maximum of 500 cycles. Given the selected mission profile, in which the aircraft will fly several flight cycles per day, this would lead to a lifetime of one battery pack to about one month. To solve this problem, batteries need to be produced at low cost. Tesla Motors and Panasonic are building huge factories (Gigafactories) around the world, in which battery packs are produced at low costs due to mass production. The factories will also have a large recycle capability for old battery cells. The industry for recycling batteries need still to be developed [28].

Table 7: Battery cell data

Due to the system voltage of 3 kV, 909 cells have to be connected in series. To reach the required capacity of 4030 kWh (see Section 4.3), 121.806 cells are needed. The maximum power is required during takeoff and initial climb. To achieve 51.2 MW from the battery pack with 3 kV, 17,067 A must be provided. This results in 170 cells connected in parallel. So not the capacity, but the maximal power extract from the battery pack determines its size with 154,530 cells. With the weight and volume of one cell, the battery pack is sized to 8,600 kg and 4.2 m³.

4.5.1 Gaseous Emissions



In order to assess future air emissions, a reference scenario and three technological scenarios are compared. S0 is the reference scenario. This describes the situation of an aircraft fleet with the current state of the art. The average annual fuel consumption would grow by + 4.4%. Considering technological progress, improved average values can be achieved in scenarios S3 and S5. The problem here is, however, that even under this consideration, the desired values for 2050 cannot be obtained according to the Global air traffic CO₂ emissions roadmap. Therefore, there is the S7 scenario where new technology is speculated. In these aspects, it is possible to reduce the growth of average annual fuel consumption to 2.3% and to achieve an annual efficiency increase of 2.0%. However, these values require a considerable investment in research. From today's point of view it is realistic to say that the improvements will settle between S5 and S7. In addition to the improved technologies, the use of alternative fuels or renewable fuel scenarios is also considered. Since alternative renewable fuels nowadays are still very expensive to manufacture, they are also classified with different mixing ratios. 10%, 30%, 50% and 100%. Combining the different technology scenarios with the classifications of the share ratios of renewable fuels, 3 life cycle reduction potentials can be established. Those 3 Life Cycle CO₂ Emissions Reduction Potentials are divided into LOW(-50%), MID(-70%), and HIGH(-90%). With the assumption that research is increasingly being conducted in the direction of renewable energy sources, the statement can be made that the aircraft creates a 90% reduction in CO₂ emissions compared to today's technology [31].

4.5.2 Noise Emissions

Due to the lack of a physical model of the aircraft, it is very difficult to make a relatively precise estimation of the noise emission. Therefore, the Boeing studies [32] based on the BOEING ERA N+2 Concept Results is used to make a first approximation. The proposed aircraft is similar to the 2025 BWB 0009A GTF. Compared to the geared turbofan concept, the lack of core engine streams and the high frequencies resulting from the very high drive speeds lead to a more efficient noise shielding. With all those advantages, we can claim that our aircraft is slightly quieter than the BWB.

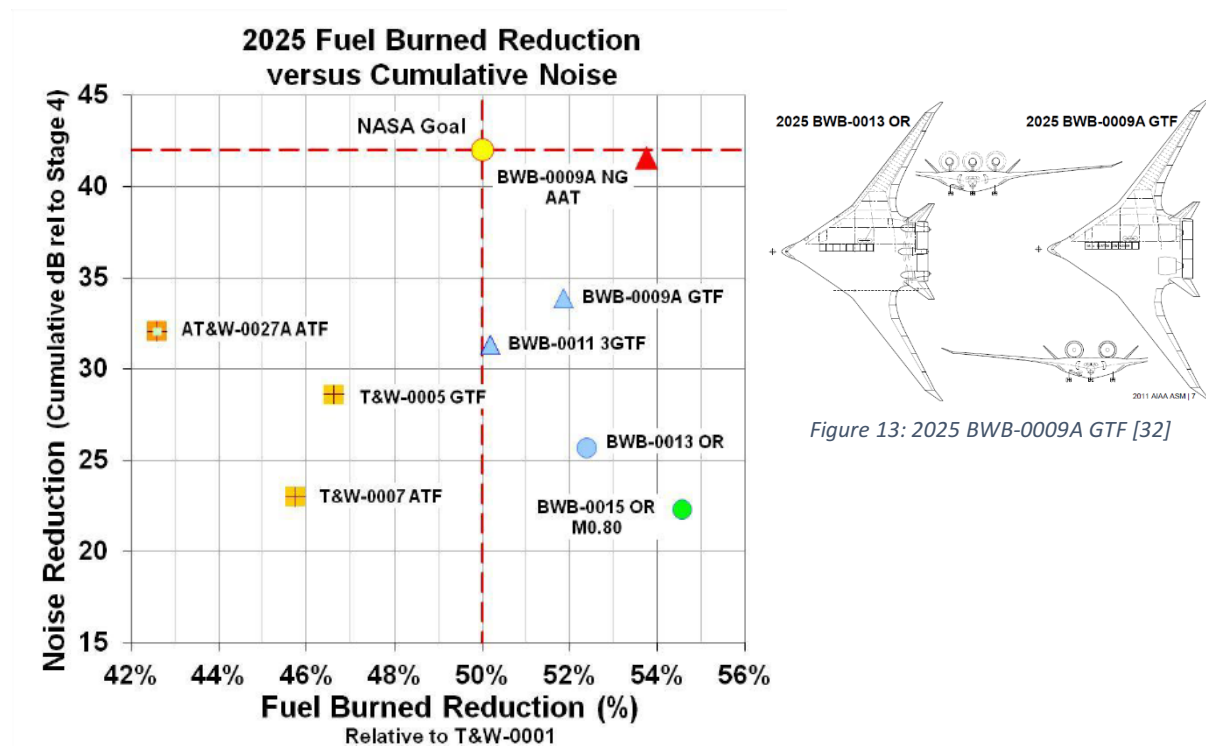


Figure 14: Noise Diagram [32]

According to [32], we can estimate the noise reduction (Cumulative dB relative to Stage 4) between 34-35 dB.

5 Cabin and Systems

5.1 System Weight and Electrical Consumption Estimation

To estimate the weight of the different aircraft systems, it was decided to take the approach with a set of formulas from Torenbeek [33] instead of using the ones that Raymer provided. This was due to the fact that Raymer's set of formulas require a lot of detailed information which was not available at this stage of the iteration process [34]. For the estimation of the dry APU weight a set of formulas by Kundu [35] was used. For the EHA weight Torenbeek's [33] estimation could not be used, as it calculated the weight of a conventional hydraulic system. Instead, an approximation based on weights of current EHA systems [7] was done. The weight of "Furnishings and Equipment" is the result of the cabin weight itself.

Considering for this project that entry-into-service will be around 2035, it is very unlikely that Torenbeek's [33] estimations from 1981 will reflect real values. For this reason, all weights but paint and emergency equipment will be factored by 0.7 due to technological advances in 54 years.

In the following table, the different system weights are listed:

Table 8: Weight of different aircraft systems

a. APU	147.70 kg
b. Instruments, Nav, Elec	4247.81 kg
c. EHA	250.00 kg
d. Electrical System	1493.80 kg
e. Furnishings and Equipment	4250.00 kg
f. Air Conditioning and Anti-Ice	386.41 kg
g. Paint and Miscellaneous	1055.00 kg
h. Emergency Equipment	1642.18 kg
Total System Weight	13472.90 kg

For a 200-passenger aircraft, like the Airbus A320, the avionics consume about 5 kW of electrical power. Since it is intended to take the flight automation to another level requiring additional computers and sensors, an estimation of 7 to 9 kW should reflect more realistic values for the aircraft. Fuel pumps and packs require another 7 kW and hydraulics 14 kW. Lighting adds in with 6 kW, de-icing with 12 kW. Heating the cabin consumes 15 to 20 kW. The enhanced inflight entertainment system requires at least an additional 20 kW. Cabin pressurization, based on B787 data, consumes around 300 kW [7]. This adds up to 390 kW, which are required during the entire flight.

Taxiing consumes 200 kW for about 15 minutes per flight. The electric energy is produced during cruise and stored in batteries. Thus, to power all electrical systems, the generators need to produce 400-450 kW of electrical power for the entire flight time.

5.2 Landing Gear: Weight and Drag reduction

The landing gear is the heaviest system of an aircraft, making up 20-27% of the entire systems weight. At the same time, it only serves a function while the aircraft is on the ground. During flight it only adds weight and drag to the equation.

Extending the gear just seconds before touchdown like the space shuttle does [36], would eliminate the problem of drag. This would require good timing by the pilots and might distract them from landing the aircraft. Also, recognizing a gear malfunction would be harder in this short time, so go-arounds might not always be possible.

For this reason the idea to automate the whole landing gear system arose. The flight computers would calculate the perfect moment to extend the landing gear, based on noise emission, physical environment, probability and consequence of extension failure. The system would also have the authority to initiate a go-around in case the gear appears to be unable to extend in time. In that case, a conventional pilot-operated gear extension could be performed for the second approach.

Weight reduction has already gone pretty far with today's technology. Since the loads a landing gear has to withstand cannot be reduced, a physical minimum of material strength and thus thickness and mass is necessary. Only the use of new materials can improve the landing gear's weight. An estimation was made that a reduction in weight of 10-15% is possible using composite materials.

The A320's main landing gear, to give a numerical example, weighs 1400 kg each, the nose gear 750 kg. With a conservative estimate of 10% in weight reduction our total landing gear weight is 3195 kg, of which 675 kg are of the nose gear. [37]

5.3 Single Pilot Operation

Some studies have been carried out on this topic, testing different methods of single pilot operation (SPO).

In a NASA study (SPO-II), simulators were set up where captains would fly standard flights alone in the cockpit, but received additional help from a virtual first officer [38] [39]. In this scenario, a so-called 'super dispatcher' works on the ground as a dispatcher and in case of upcoming problems in the cockpit, he receives real-time data from the aircraft. This is then displayed in a second "cockpit", a ground station receiving the exact kind of data the in-air pilot receives as well. A video chat connection between captain in the actual aircraft and first officer on the ground is established as well. That way, the two pilots could theoretically work together as if they were in one cockpit together.

Some advantages of this system: During low work load in the real cockpit, the virtual first officer is not necessary and can help other captains in other aircraft [40]. That way one virtual first officer can replace numerous real ones, switching between the airplanes that need his assistance. Furthermore, no real technological advancement is needed. This concept would work in regular 2-crew cockpits, with the first officer simply disappearing whenever he is not needed.

During simulations of this principle however, it turned out that virtual first officers often lacked a proper level of situational awareness, because they found themselves in sometimes eight to ten different scenarios within a short period of time, mixing up flight details or the tasks that were delegated to them by different captains. Another problem was simply caused by the lack of communication, by not knowing 'what the other one was doing'.

Also, this method relies heavily on a stable datalink between ground and airplane. In an emergency situation, where help by a virtual first officer is needed the most, it is not unlikely that the corresponding systems might be damaged or in any other way inoperative.

A more realistic approach to SPO is to replace the first officer with technology. Just like modern navigation equipment, onboard computers, and digital engine control made the flight engineer obsolete, typical "pilot monitoring" tasks, such as radio operation, flight parameter surveillance, checklist read backs etc. can all be automated, even with today's technology. In fact, NASA has been working on a project since 2006 which one day is supposed to make the whole area of air traffic control obsolete [41]. Aircraft would simply communicate with each other, predicting future aircraft movements better than any human ATC could, and thus guide themselves around the airspace. With ATC, route planning and monitoring, as well as visual collision avoidance being a thing of the past, a big part of a pilot's everyday workload disappears and the remaining workload might as well be small enough to be handled by only one pilot.

As far as technology goes, SPO should be a realistic option by at least 2035. The main argument against SPO is the topic on human factors. A single pilot in the cockpit might get bored more easily, having a bad influence on the pilot's vigilance. In case of an emergency, where the pilot must take the aircraft over from the autopilot, there is no help, no backup and no instance that could detect a mistake.

For this reason, it might be more realistic to keep 2 pilots in the cockpit for another few decades and then, as technology advances furthermore, eliminate the human factor out of the equation altogether. Since this is still a thing of the future, and SPO needs to be studied much more closely before the first SPO aircraft can be built, no final conclusion regarding this specific aircraft can be drawn.

5.4 Cabin, In-Flight Entertainment and Cabin Crew

The configuration of the aircraft includes a relatively flat lower fuselage surface in combination with a round, circular upper half. Therefore, a regular cabin layout does not fit into the intended fuselage design. Keeping the aircraft's mission in mind, short haul flights between medium sized cities, a large baggage compartment becomes obsolete. As a result, the cabin floor can be placed close to the lower end of the fuselage, leaving just enough room for the systems. Thus, a large space between cabin ceiling and the upper end of the fuselage emerges with just the perfect size to accommodate a second cabin.



Figure 15: Cross section of the cabin

The result is 21 rows with a total of 14 seats each which accommodate 294 passengers in 3 separate cabins on two decks. The reason for splitting the lower cabin into two compartments lies once again in the intended mission. The aircraft is supposed to fly between small to medium size cities in Asia, acting as a regional transit. Multistop routes will be a common occurrence for this aircraft. Having three separate cabins, the operator can fill the cabins based on a group of passenger's final destination, eliminating the need for boarding and deboarding the whole aircraft with every turn-around. As far as the ground handling is concerned, the 3-cabin aircraft can be viewed as an 80-seat regional aircraft at every stop. Furthermore, the operator has the ability to fit every cabin with a different product: one cabin economy class, another cabin premium economy, for example. The flexibility of this configuration is unique.

Trying to reduce structural weight, it was decided to construct the fuselage without windows and install large LED-screens for every row, imitating the view out of a large window [42] [43]. Whether an actual live feed from the outside or an artificial scenery is shown, is up to the operator. This not only saves weight, but collaborates perfectly with our 3-cabin design. Passengers sitting next to the inner wall will feel like they have a window seat instead. From every cabin's perspective, the airplane is much smaller and more private than it actually is.

But these screens not only serve as window-replacements, they can also be used as a personal IFE system for every passenger, they can include the menu for the on-board shop, which allows passengers to have snacks and beverages automatically delivered to their seats through a vending machine-like apparatus behind the cabin walls, and most importantly, the screens can support the flight attendants during an emergency situation:

Should a passenger become sick during flight, a live-feed to an airline's on ground on-duty doctor can be established through the "window"-screen, should an airline support this system. Video tutorials with

instructions for the most common medical conditions onboard airplanes, however, will be included as well. In case of an emergency evacuation, the screens not only help illuminate the cabin despite possible thick smoke, they will also indicate the direction and distance in rows to the nearest exit.

The minimum required number for cabin crew is six for 300 passengers [44]. Also, six emergency exits are required [45] [46]. Keeping in mind that flight attendants are not required as service providers anymore, they only serve a safety function: attending passengers with sudden medical issues and assisting during evacuations. For both cases, improvements have been implemented compared to today's standards (live video chat with doctors, common illustrations for first-aid, illumination and indications to nearest exit during evacuation), meaning that a reduction in cabin crew to 4 can be justified, without reducing the statistical safety required by certification standard below today's level [44].



Figure 16: LED Screens and Seats (lower-deck)

5.5 Electric taxiing

In 2011, a study by DLR and Airbus was carried out, which tested both a fuel cell and the APU as power sources for an electrical taxiing system [47]. For older aircraft or even newer aircraft of an older generation (e.g. A320ceo and neo), the (retro-) fitting of such a system almost never appears economically viable. Keeping in mind that the propulsion system relies heavily on an electrical system, the implementation of an electrical taxi system is the next logical step. The only additions necessary to the electric propulsion system are electric motors, weighing not more than 70 kg for each main gear. The rest of the electric infrastructure is already present. Since there is no need for the engines to run for taxi, taxi fuel becomes obsolete. The net result is a taxi weight lower than without the electric taxi system [48] [49].

Additionally, the landing gear will be designed in such a way that it will withstand even longer towing procedures directly to and from the runway [50]. Corresponding systems are already being tested, like the fully automated "taxibot", used in cooperation with Lufthansa's B737 at Frankfurt Airport [51] [52] [53]. Using a system like this whenever possible makes overall operations even more fuel and noise efficient [54]. Whenever a taxibot is not available, the electrical taxiing system does the job.

5.6 Environmental Control Unit

Due to the specific mission of the proposed aircraft, most of the time it will operate in lower altitudes than comparable airplanes. Thus, the pressure difference it needs to maintain is significantly smaller than usual. Using bleed air for cabin pressurization and air conditioning would decrease the propulsion system's efficiency, which cannot be accepted. Therefore, it was decided to go with an electric compressor, similar to the B787 system, allowing for fuel savings of up to 3% [55].

6 Weight and Balance

6.1 Wing Structure

To define the weight of the wing, the maximum bending moment of the wing had to be identified.

The lift of the wing and of the C-wing, structural weight of the wing due to boron-epoxy material, additional 20% structural weight because of the C-wing, as well as fuel and landing gear stored in the wing were considered to calculate the maximum moment for a conventional wing. To adapt this to a semi-blended wing, a moment reduction of 20% was applied [56].

To compensate the bending moment, two I-beam spars made from a boron epoxy composite were integrated in each wing. The sizing of the I-beams was done using a cantilever beam calculation.

The total structural weight of the wing was thus calculated to be 12.480 kg.

6.2 Fuselage Structure

The calculations to define the weight of the fuselage were based on formulas presented by Corke [51] for conventional aircrafts, which relate the geometry and components to the weight:

$$W_{\text{fuse}} = C_1 C_2 C_3 W_{\text{dg}}^{C_4} n^{C_5} L^{C_6} L_t^{C_7} D^{C_8} S_f^{C_9} W^{C_{10}} (1 + K_{ws})^{C_{11}} q^{C_{12}} + C_{13} \quad [57]$$

For transport aircraft:

$$C_1 = 0.328$$

$$C_2 = K_{\text{door}} = 1$$

$$C_3 = K_{\text{lg}} = 1$$

$$C_4 = 0.5$$

$$C_5 = 0.5$$

$$C_6 = 0.35$$

$$C_7 = 0$$

$$C_8 = -0.1$$

$$C_9 = 0.302$$

$$C_{10} = 0$$

$$C_{11} = 0.04 \quad C_{12} = 0$$

$$C_{13} = 0$$

W_{dg} = design gross weight

n = design load factor

L = length of fuselage

L_t = length between c/4 locations of Main Wing and H-Stabilizer

D = maximum height or effective diameter

S_f = Fuselage wetted area

W = maximum width or effective diameter

$$K_{ws} = 0.75 [(1+2\lambda)/(1+\lambda)] [(b_w/L)\tan\Lambda]$$

b_w = main wingspan

q = dynamic pressure at cruise

The results of this calculation were modified by applying increasing factors for the oval shape (20% [56]) and for the airfoil shape (21%).

The total fuselage weight was calculated to be 13530 kg.

6.3 CG and MTOM Calculation

To identify the center of gravity, a point mass approach was used:

$$R = \frac{1}{M} \sum_{i=1}^n m_i r_i$$

M = total mass

n = number of components

m_i = component mass

r_i = location of component CG

Given the weight and position of each component as summarized in Table 9, the gross weight and the overall CG position was calculated.

Table 9: Calculation Center of Gravity

	m _i [kg]	x _i [m]	m _i x _i [kg·m]
APU	147.7	23	3397.1
Instruments, Nav, Elec	4247.81	1	4247.81
Hydraulics, Pneumatics	250	10	2500
Electrical System	1493.8	10	14938.02
Furnishings, Equipment, People	28250	13.05	368662.5
A/C and Anti-Icing	386.4	12	4636.8
Paint and Misc.	1055	19	20045
Emergency Equipment	1642.18	4	6568.73
Main Landing Gear	2520	16.32	41126.4
Nose Landing Gear	675	2.5	1687.5
Fans	3000	26	78000
Turbo generators	1500	26	39000
Fuel	10500	18	189000
Generator	850	28	23800
Electric Motor	4800	26	124800
Inverter	3800	27	102600
Battery	8600	7	60200
Cable	500	15	7500
Power electronics	3300	7	23100
Thermal management system	2500	15	37500
Wing	12478.78	18	224618.09
Fuselage	13527.64	16.6	224558.76
Empennage	2000	30	60000
Gross Weight	108024.3		1662486.7
Total CG:			15.39 m
			45.265 %

All in all, the maximum take-off mass is 108 tons. The center of gravity is at 15.4 m measured from nose (around 45% of fuselage length).

7 Conclusion

The aircraft meets the requirements for flight path 2035 easily. The aerodynamic shape allows L/D of 25 with great climb performance. The laminar flow is very pronounced through the wing airfoils and the carbon fiber material. Morphing structures and boundary layer suction increase the efficiency and reduce the noise emission. A new system for the landing gear decreases the noise emission in the final approach. Through all these effects the noise reduction requirements are reached. The new fuselage requires a new cabin layout which allows fast boarding and deboarding with high comfort and safety.

The propulsion system is unlike any used for aircrafts today. Gas turbines drive generators which provide electrical energy. Electrically driven ducted fans mounted on the top rear part of the fuselage provide thrust. The engines are perfectly shielded in the fuselage, and the ducted fans are shielded by small vertical stabilizers. With the very efficient intercooled recuperative turbo generators running in the design point for the whole flight, a fuel burn less than 1.27 kg per 100 km per PAX is reached, which is an improvement of 33.2 % compared with a Boeing 737-900ER from 2006. By using bio fuels the required life-cycle CO₂ savings are achievable and by using a cryocooled electric system, further enhancements in fuel burn are possible. With a lean prevaporized premixed combustion chamber a NO_x reduction of 90 % is reached. Furthermore, carbon fiber materials and 3D printed components decrease the structure weight thereby the fuel consumption.

The three-view of the proposed concept is shown below in Figure 17.

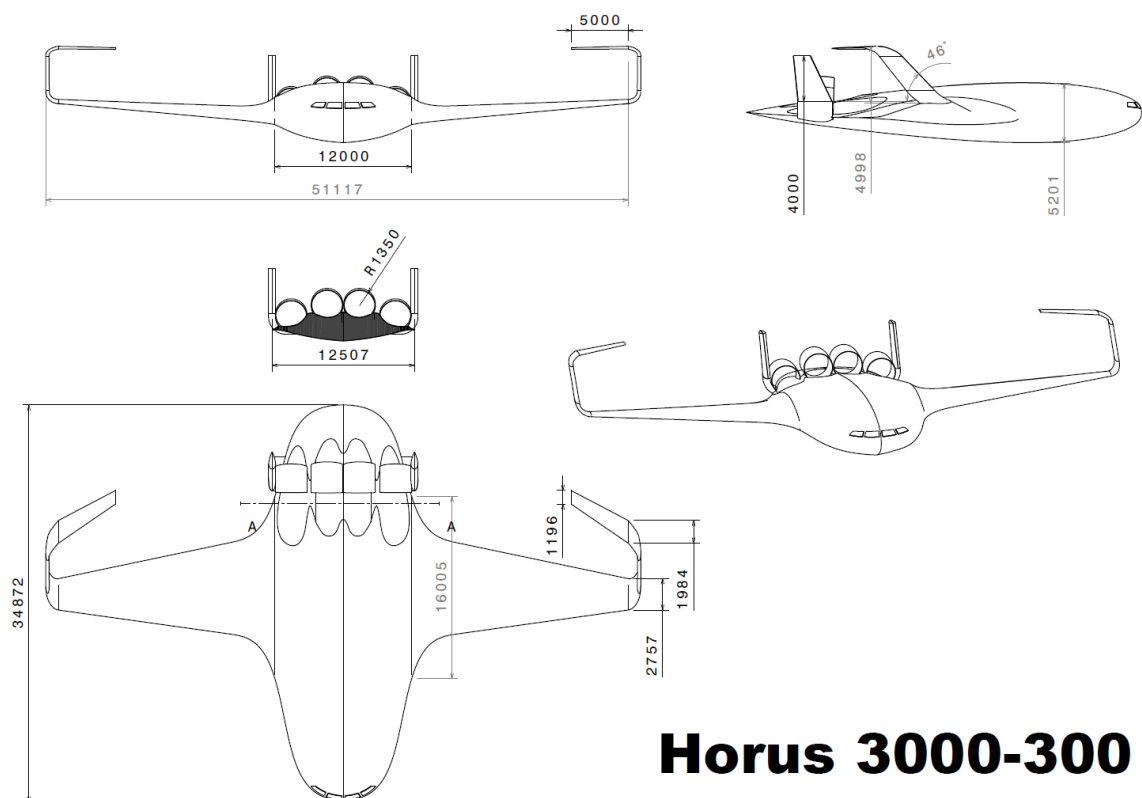
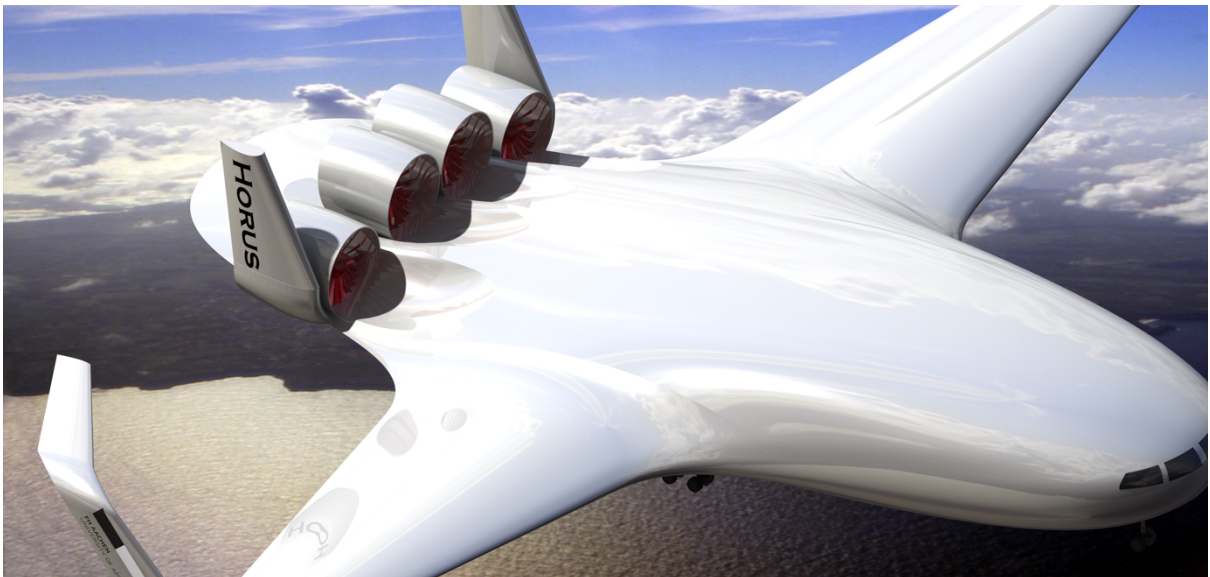


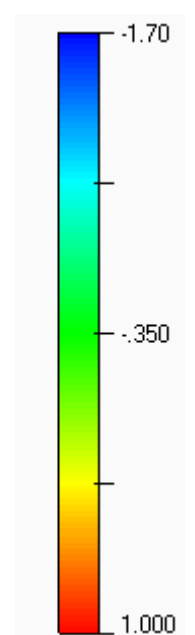
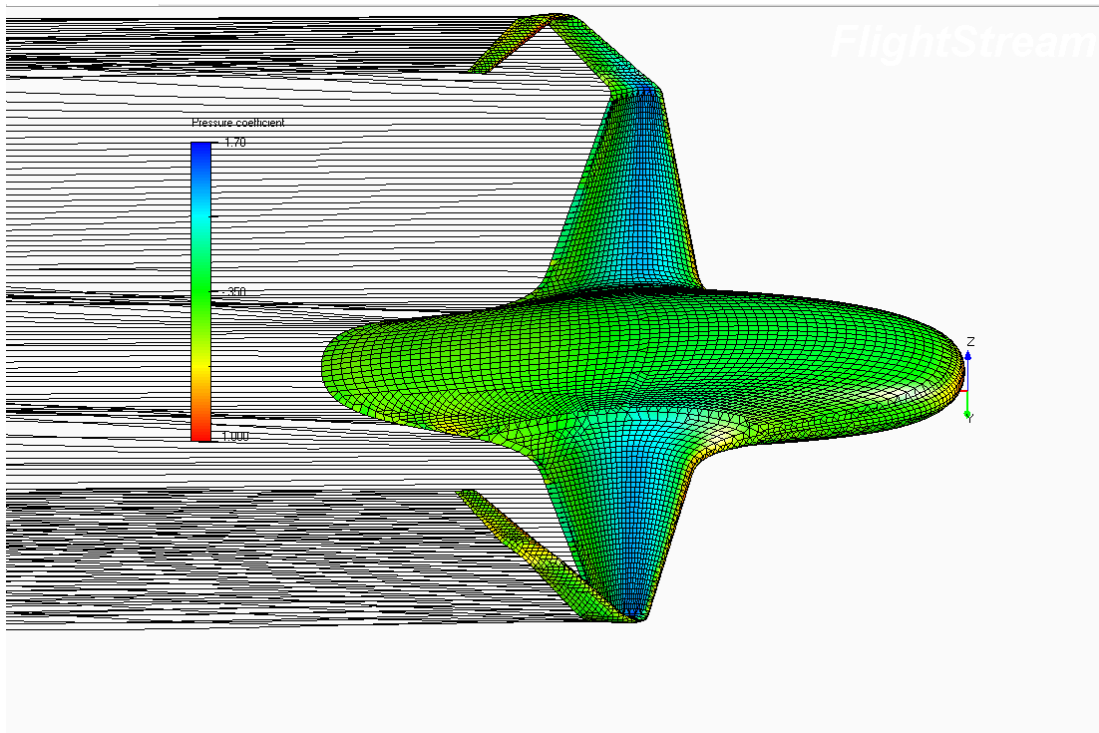
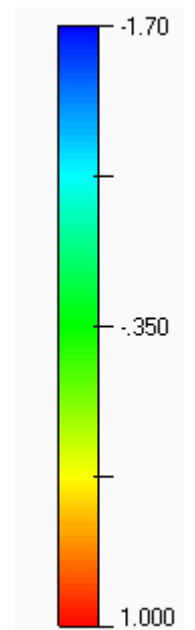
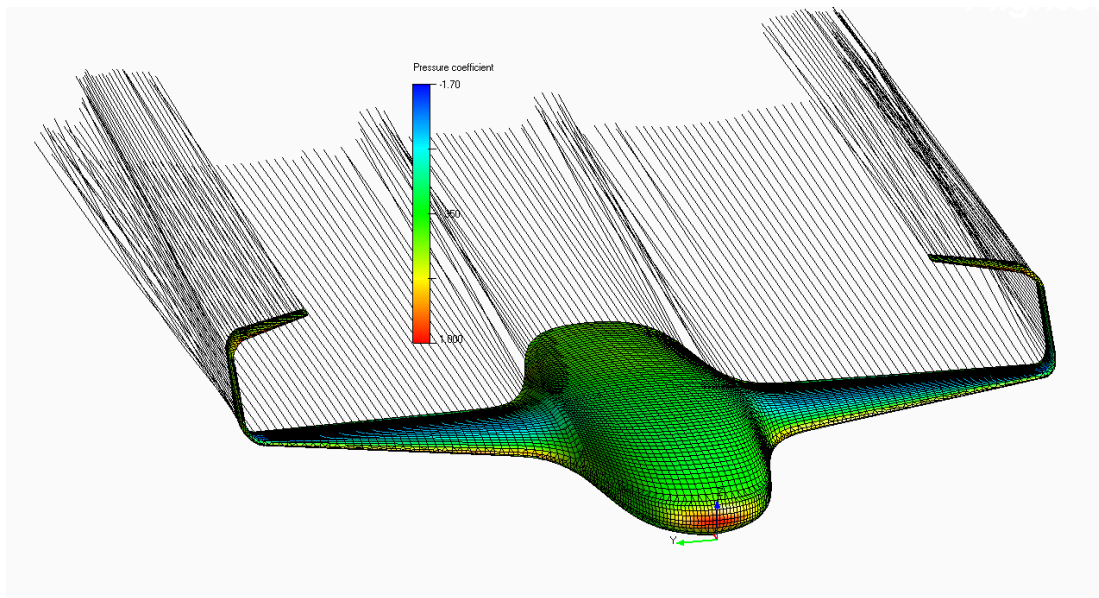
Figure 17: Three view drawing

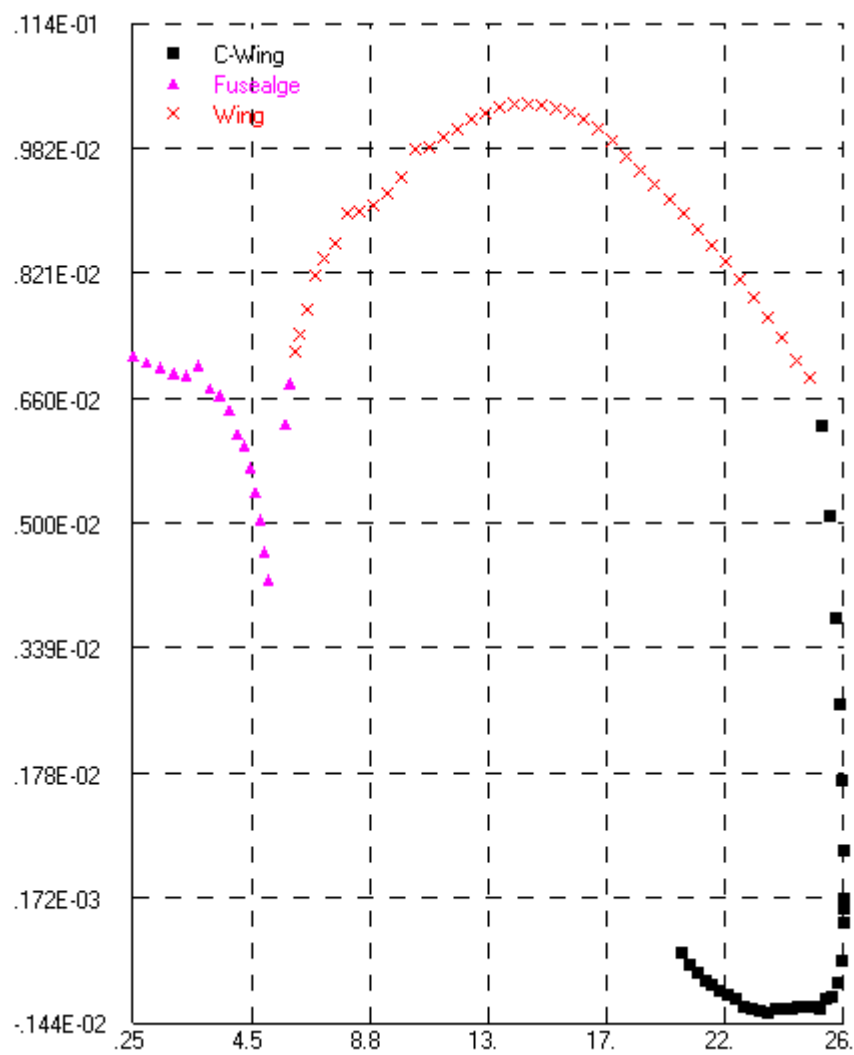
Appendix

Model Pictures

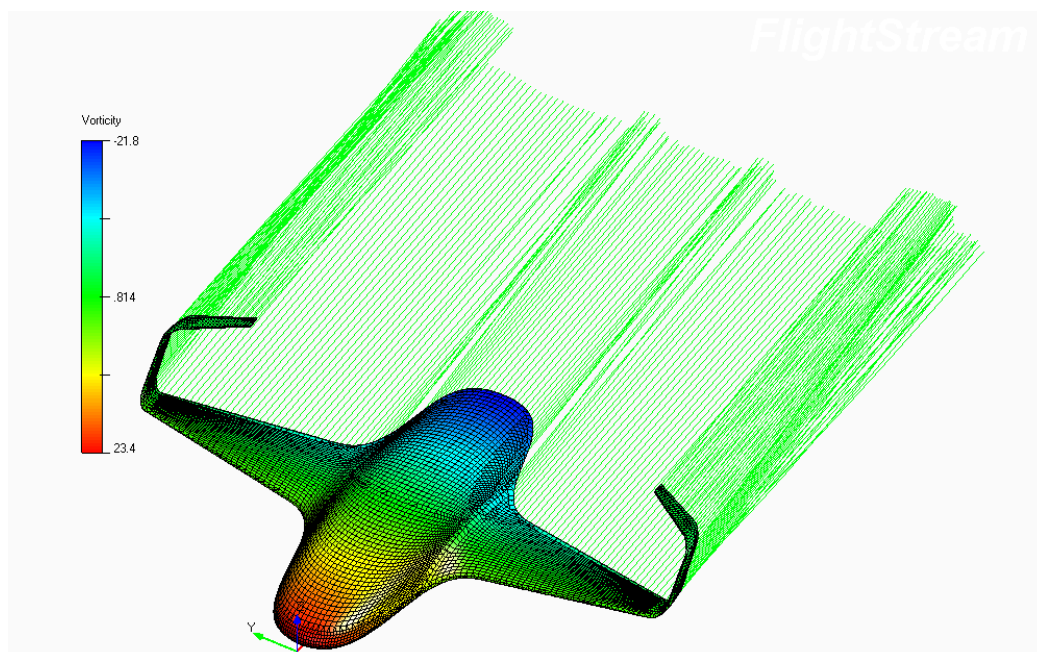


Pressure distribution





Vorticity



Bibliography

- [1] T. E. Online, "Daily Chart - Top Flights," 15 08 2014. [Online]. Available: <http://www.economist.com/blogs/graphicdetail/2012/05/daily-chart-8>. [Accessed 25 06 2017].
- [2] T. A. Reist, "High-Fidelity Aerodynamic Shape Optimization of a Lifting-Fuselage Concept for Regional Aircraft," Troronto, Ontario, 2016.
- [3] McGowan, Washburn, Horta, Bryant, Cox, Siochi, Padula and Holloway, Recent Results form NASA's Morphing Projekt, NASA Langley Research Center, Hampton, VA.
- [4] I. Kroo, J. McMasters and S. C. Smith, "Highly Nonplanar Lifting Systems," NASA Ames Research Center, 2000.
- [5] D. S. Karan Bikkanaavar, "Inestigation and design of a C-Wing passenger aircraft," Hamburg, Germany ; Wichita, USA, 2016.
- [6] S. A. Ning and I. Kroo, "Tip Extensions, Winglets, and C-Wings: Conceptual Design and Optimiszation," Stanford University, CA, USA, 2008.
- [7] Prof. Dr. C. Braun, Systemintegration, FH Aachen, 2014.
- [8] D. P. Raymer, Aircraft Design: A Conceptual Approach, Washington DC: American Institute of Aeronautics and Astronautics, 1992, pp. 280-290.
- [9] Prof. Dr.-Ing. C. Braun, Aircraft Design 1, Aachen, 2015.
- [10] climate4you, "climate4you," [Online]. Available: www.climate4you.com. [Accessed 19 06 2017].
- [11] N. E. a. Fuel, "New Energy and Fuel," 19 06 2017. [Online]. Available: <http://newenergyandfuel.com/http://newenergyandfuel.com/2009/05/06/storing-energy-the-terms-and-the-payoff-to-consumers/energy-density-specific-energy-graph/>. [Accessed 19 06 2017].
- [12] "Spektrum," 19 06 2017. [Online]. Available: <http://www.spektrum.de/news/energiewende-mit-algen-zu-sauberer-energie/1352317>.
- [13] R. A. McDonald, "Electric Propulsion Modeling for Conceptional Aircraft Design".
- [14] Lengyel-Kampmann, Voß, Niecke, Rüd and Schaber, "GENERALIZED OPTIMIZATION OF COUNTER-ROTATING AND SINGLE-ROTATING FANS," in *ASME Turbo Expo 2014: Turbine Technical Conference and Exposition*, Düsseldorf, Germany, 2014.
- [15] H. Gunn, "AERODYNAMICS OF BOUNDARY LAYER INGESTING FANS," in *ASME Turbo Expo 2014: Turbine Technical Conference and Exposition*, Düsseldorf, Germany, 2014.
- [16] G. V. Brown, "Weights and Efficiencies of Electric Components of a Turboelectric Aircraft Propulsion System," in *49th AIAA Aerospace Sciences Meeting including the New Horizons Forum and Aerospace Exposition*, Orlando, Florida, 2011.
- [17] C. Liu, Turboelectric Distributed Propulsion System Modelling, C. UNIVERSITY, Ed., 2013.

- [18] J. L. Felder, H. D. Kim, G. V. Brown and J. Chu, "An Examination of the Effect of Boundary Layer Ingestion on Turboelectric Distributed Propulsion Systems," American Institute of Aeronautics and Astronautics.
- [19] J. Felder, M. Tong and J. Chu, "Sensitivity of Mission Energy Consumption to Turboelectric Distributed Propulsion Design Assumptions on the N3-X Hybrid Wing Body Aircraft," in *48th AIAA/ASME/SAE/ASEE Joint Propulsion Conference 2012*, Atlanta, Georgia, 2012.
- [20] R. Fink, Untersuchungen zu LPP-Flugtriebwerksbrennkammern unter erhöhtem Druck, München: Technischen Universität München, 2001.
- [21] C. F. McDonald, A. F. Massardo, C. Rodgers and A. Stone, "Recuperated gas turbine aeroengines, part II: engine design studies following early development testing," *Aircraft Engineering and Aerospace Technology*, no. 80, 2008.
- [22] H. Gonser, Untersuchungen zum Einsatz von Wärmetauschern in zivilen Turboflugtriebwerken, Stuttgart: Institut für Luftfahrtantriebe der Universität Stuttgart, 2008.
- [23] D. J. R. Welstead and J. L. Felder, "Conceptual Design of a Single-Aisle Turboelectric Commercial Transport with Fuselage Boundary Layer Ingestion".
- [24] F. Lambert, "Tesla starts mass production of new '2170' battery cell at the Gigafactory, will be used in Model 3 in Q2," 04 01 2017. [Online]. Available: <https://electrek.co/2017/01/04/tesla-2170-battery-cell-production-gigafactory-model-3/>. [Accessed 24 06 2017].
- [25] S. E. C. L. Portable Rechargeable Battery Business Division, "www.akkuplus.de," [Online]. Available: http://akkuplus.de/mediafiles/Datenblatt/Panasonic/Panasonic_NCR20650A.pdf. [Accessed 22 06 2017].
- [26] VW, "www.elektromobilität.nrw.de," [Online]. Available: http://www.elektromobilitaet.nrw.de/fileadmin/Daten/Download_Dokumente/Batterien_als_elementarer_Bestandteil_zukuenftiger_Antriebstechnik-Dr._Loesche-ter_Horst.pdf. [Accessed 22 06 2017].
- [27] Birke and Prof. Dr.-Ing. Kai Peter, "Li-Ion and Post Li-Ion – From theoretical to usable energy densities," in *Batterietagung 2016*, Münster, Germany, 2016.
- [28] Zeit, "www.zeit.de," [Online]. Available: <http://www.zeit.de/mobilitaet/2016-11/batterie-recycling-elektroauto-speicher-stromnetz/seite-2>. [Accessed 22 06 2017].
- [29] X. Xue, Y. Lin, C. Zhang, Y. Tian and C.-J. Sung, "EXPERIMENTAL STUDY ON NOX AND CO EMISSIONS OF AVIATION KEROSENE AND COAL-TO-LIQUID SYNTHETIC AVIATION FUEL IN A JET STIRRED COMBUSTION REACTOR," in *Proceedings of ASME Turbo Expo 2014: Turbine Technical Conference and Exposition*, Düsseldorf, Germany, 2014.
- [30] [Online]. Available: https://en.wikipedia.org/wiki/Fuel_economy_in_aircraft. [Accessed 26 06 2017].
- [31] F. Wolters, M. Schaefer and R. v. d. Bank, "POTENTIAL IMPACT OF RENEWABLE FUELS AND TECHNOLOGICAL INNOVATIONS ON GLOBAL AIR TRAFFIC EMISSIONS DEVELOPMENT BY 2050," in *Proceedings of ASME Turbo Expo 2014: Turbine Technical Conference and Exposition*, Düsseldorf, Germany, 2014.
- [32] J. T. Bonet, "Boeing ERA N+2 Advanced Vehicle Concept Results," 2012.

- [33] E. Torenbeek, *Synthesis of Subsonic Airplane Design: An introduction to the preliminary design of subsonic general aviation and transport aircraft, with emphasis on layout, aerodynamic design, propulsion and performance*, Delft: Delft University Press, 1988.
- [34] O. Al-Shamma and Dr. A. Rashid, "Aircraft weight estimation in interactive design process," 2013.
- [35] A. K. Kundu, *Aircraft Design*, Cambridge University Press, 2010.
- [36] NASA, "Main Shuttle Crew OPs Manual," 2008.
- [37] Airbus, "Flight Crew Operating Manual," 2000.
- [38] J. Lachter, L. Brandt, V. Battiste, S. Ligda, M. Matessa and W. Johnson, "Toward Single Pilot Operations: Developing a Ground Station," 2014.
- [39] D. Comerford, S. L. Brandt, J. Lachter, S.-C. Wu, R. Mogford, V. Battiste and W. W. Johnson, "NASA's Single-Pilot Operations Technical Interchange Meeting: Proceedings and Findings," 2013.
- [40] D. Bilimoria, W. Johnson and P. Schutte, "Conceptual Framework for Single Pilot Operations," 2014.
- [41] D. Communications, Director, *Mayday Alarm im Cockpit - Risikofaktor Autopilot*. [Film]. Kanada.2008.
- [42] ICAO, "Ready for big-screen TV Airplanes?," *ICAO Journal Vol. 70, No. 1*, vol. 70, no. 1, p. 40, 2015.
- [43] S. Bagassi, F. Lucci and F. Persiani, "Aircraft Preliminary Design: a windowless concept," University of Bologna – DIN, Industrial Engineering Department, 2015.
- [44] European Commission, "COMMISSION REGULATION (EU) No 965/2012," 2012.
- [45] EASA, "Acceptable Means of Compliance (AMC) and Guidance Material (GM) to Annex III – Part-ORO," 2016.
- [46] EASA, "EASA Safety Information Bulletin 2014-29 (Draft)," 2014.
- [47] DLR, "DLR Airbus A320 ATRA taxis using fuel cell-powered nose wheel for the first time," 06 07 2011. [Online]. Available: http://www.dlr.de/dlr/en/desktopdefault.aspx/tabid-10204/296_read-931/#/gallery/2079. [Accessed 19 06 2017].
- [48] S. Steinke, "Airbus A320: Rolltest mit elektrischem Antrieb," Motor Presse Stuttgart GmbH & Co. KG, 2011. [Online]. Available: <http://www.flugrevue.de/zivilluftfahrt/flugzeuge/airbus-a320-rolltest-mit-elektrischem-antrieb/490558>. [Accessed 17 06 2017].
- [49] S. Steinke, "Honeywell und Safran lassen A320 elektrisch rollen," Motor Presse Stuttgart GmbH & Co. KG, 2011. [Online]. Available: <http://www.aero.de/news-13946/39.html>. [Accessed 17 06 2017].
- [50] BBC, "Virgin Atlantic move to save fuel," BBC, 03 12 2006. [Online]. Available: <http://news.bbc.co.uk/2/hi/business/6203636.stm>. [Accessed 19 06 2017].
- [51] TaxiBot, "TaxiBot Concept," [Online]. Available: <http://www.taxibot-international.com/concept>. [Accessed 19 06 2017].
- [52] TLD, "INNOVATIVER TAXIBOT JETZT IM EINSATZ IN REALEM FLUGBETRIEB," 02 03 2015. [Online]. Available: <https://www.tld-group.com/de/nachrichten/innovativer-taxibot-jetzt-im-einsatz-realem-flugbetrieb/>. [Accessed 19 06 2017].

- [53] C. Alcock, "TaxiBot Ready To Cut Cost and Carbon Footprint for Taxiing," 10 10 2016. [Online]. Available: <http://www.ainonline.com/aviation-news/air-transport/2016-10-10/taxibot-ready-cut-cost-and-carbon-footprint-taxiing>. [Accessed 19 06 2017].
- [54] S. B. Katja Hein, "ACOUSTICAL COMPARISON OF CONVENTIONAL TAXIING AND DISPATCH TOWING – TAXIBOT'S CONTRIBUTION TO GROUND NOISE ABATEMENT," 2016.
- [55] M. Sinnett, "787 No-Bleed Systems: Saving Fuel and enhancing operational efficiencies," Boeing Press Release, Everett, 2007.
- [56] R.H.Liebeck, "Design of the Blended Wing Body Subsonic Transport," *Journal of Aircraft*, January-February 2004.
- [57] T. C. Corke, Design of Aircraft, Prentice Hall, 2002.

FH Aachen | Postfach 10 05 60 | 52005 Aachen

Dr. Klausdieter Pahlke

Deutsches Zentrum für Luft- und Raumfahrt
Programmdirektion Luftfahrt
Tel.: +49 531 295-3270

Dr. Olaf Brodersen

Deutsches Zentrum für Luft- und Raumfahrt
Institut für Aerodynamik und Strömungstechnik
Tel.: +49 531 295-2445

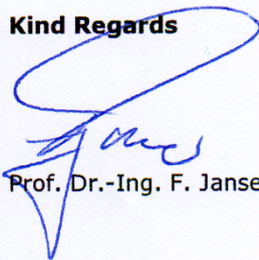
Attestation for Submission

Dear Dr. Pahlke, dear Dr. Brodersen,

the Department of Aerospace Engineering of the FH Aachen - University of Applied Sciences hereby certifies that the report of the NASA / DLR Design Challenge team has been approved and agreed by us. The related work has been developed and conducted by the student team without any further support of our academic staff.

The submission to the NASA / DLR Design Challenge is supported.

Kind Regards



Prof. Dr.-Ing. F. Janser

FH Aachen
Hohenstaufenallee 6
52064 Aachen
www.fb6.fh-aachen.de

Ansprechpartner

Prof. Dr.-Ing.
Frank Janser
Dipl.-Ing.
Rolf Schauer

Fachbereich

Luft- und Raumfahrttechnik

Lehrgebiet

Strömungsmechanik,
Aerodynamik

Kontakt

T +49. 241. 6009 52308
F +49. 241. 6009 52834
Schauer@fh-aachen.de

Datum

27.06.2017

Verzeichnis der Mitglieder des Teams der FH Aachen University of Applied Sciences inkl. Fachsemesterzahl und Postadressen

	Name	Vorname	Studienfach	Fachsemester	Straße + Hausnummer	PLZ	Ort
1	Bergmann	Ole	Luft- und Raumfahrttechnik B. Eng	6	Jakobstraße 25a	52064	Aachen
2	Bremen	Jan Frederik	Luft- und Raumfahrttechnik B. Eng	6	Benediktinerstraße 32	52066	Aachen
3	Franke	Christian	Aerospace Engineering M. Sc.	2	Zollernstraße 25	52070	Aachen
4	Hardt	Daniel	Luft- und Raumfahrttechnik B. Eng	6	Van-Brandis-Straße 12	52064	Aachen
5	Heitsch	Christina	Luft- und Raumfahrttechnik B. Eng	6	Taubenstraße 23	42699	Solingen
6	John	Yohan	Aerospace Engineering M. Sc.	2	Schillerstrasse 88	52064	Aachen
7	Licht	Benjamin	Aerospace Engineering M. Sc.	1	Reumontstraße 40	52064	Aachen
8	Möhren	Felix	Luft- und Raumfahrttechnik B. Eng	6	Tieloh 59	22307	Hamburg
9	Muñoz	Carolina	Aerospace Engineering M. Sc.	3	Marienbongard 26	52062	Aachen
10	Plante	Robert	Luft- und Raumfahrttechnik B. Eng	8	Viktoriastraße 64	52066	Aachen
11	Rommeler	Johannes	Aerospace Engineering M. Sc.	3	Karlsgraben 69	52064	Aachen
12	Schreiber	Philip	Aerospace Engineering M. Sc.	2	Wendinger Str. 5	57258	Freudenberg
13	Schwabroch	Carsten	Aerospace Engineering M. Sc.	1	Mariabrunnstr 49	52064	Aachen
14	Weber	Darius	Luft- und Raumfahrttechnik B. Eng	6	Hohenstaufenallee 18	52064	Aachen